buildings

MDPI

Article

Preliminary Reactivity Test for Precursors of Alkali-Activated Materials

Sâmara França [1], Leila Nóbrega Sousa [2], Marcos Vinicio de Moura Solar Silva [3], Paulo Henrique Ribeiro Borges [1] and Augusto Cesar da Silva Bezerra [4,*]

[1] Department of Civil Engineering, Federal Center for Technological Education of Minas Gerais, Belo Horizonte 30421-169, Brazil
[2] Department of Materials Engineering, Federal Center for Technological Education of Minas Gerais, Belo Horizonte 30421-169, Brazil
[3] Energy Company of Minas Gerais, Belo Horizonte 30190-131, Brazil
[4] Department of Transport Engineering, Federal Center for Technological Education of Minas Gerais, Belo Horizonte 30421-169, Brazil
* Correspondence: augustobezerra@cefetmg.br; Tel.: +55-31-3319-7119

Abstract: Alkali-activated materials (AAMs) result from the dissolution process and polycondensation of precursors in high pH solutions. This material is considered alternative cement with similar properties and lower environmental impact than Portland cement. However, AAMs are subjected to the same standardization applied to cement-based materials since no formal methods exist to characterize this material and/or the precursor reactivity. Therefore, this work aims to develop a method to characterize the reactivity of the main precursors used to produce AAMs. Hence, the precursors were assessed in two steps after chemical, physical, and mineralogical characterization. The first step evaluated the crystallinity change of the material after the acid attack by mixing 1 g of each material in 100 mL of 1% HF solution for 6 h at ambient temperature. The crystallinity change was evaluated by comparing the X-ray diffraction of the materials before and after the acid attack. The second step involved evaluating the formation of geopolymerization products in the pastes of studied precursors through FTIR test. The pastes were produced with Na_2SiO_3 and NaOH as activators. After 28 days of curing, the pastes were submitted to a FTIR test for structural analysis. This method was tested evaluating the reactivity of traditional precursors for alkali activation (i.e., silica fume (SF), blast furnace slag (BFS), and metakaolin (MK)), in addition sugarcane bagasse ash mechanically treated (SCBAM) and sugarcane bagasse ash mechanically and heat treated (SCBAMH) since SCBA is a promising precursor for alkali activation. Considering the crystallinity change of precursors (step 01), the formation of geopolymerization products (step 02), and the chemical composition of precursors (preliminary characterization), it could be concluded that: (i) surface area is not relevant to materials with small particle size (<23 μm); (ii) amorphous area is only relevant if the material exhibits the optimal chemical composition; and (iii) the chemical composition is a crucial parameter for alkali activation. In addition, the potential precursors for alkali activation should have a significant amorphous halo and a SiO_2/Al_2O_3 ratio of 2 to 5. Also, it could be concluded that SF and SCBAMH do not exhibit adequate reactivity while BFS, MK, and SCBAM can be classified as reactive precursors.

Keywords: reactivity; precursors; alkali-activated materials; sugarcane bagasse ash; chemical composition; surface area; crystallinity

check for updates

Citation: França, S.; Sousa, L.N.; Silva, M.V.d.M.S.; Borges, P.H.R.; Bezerra, A.C.d.S. Preliminary Reactivity Test for Precursors of Alkali-Activated Materials. *Buildings* **2023**, *13*, 693. https://doi.org/10.3390/buildings13030693

Academic Editor: Elena Ferretti

Received: 2 February 2023
Revised: 20 February 2023
Accepted: 1 March 2023
Published: 6 March 2023

Copyright: © 2023 by the authors. Licensee MDPI, Basel, Switzerland. This article is an open access article distributed under the terms and conditions of the Creative Commons Attribution (CC BY) license (https://creativecommons.org/licenses/by/4.0/).

1. Introduction

Civil construction is directly linked with the economy of countries and social growth. The consumption of buildings material in developing countries is more expressive owing to the highest demands for civil construction infrastructure. It is estimated that the cement consumption in the world is about 450 kg per capita, and therefore cement is the most

demanded building material globally [1]. This consumption tends to increase since it is estimated that the world population in 2050 should be 9.8 billion, and 68% of this total should live in urban areas. In 2020, the population increased to 7.8 billion, with nearly 55% living in urban areas [2].

At the same time, the cement industry exhibits a wide impact on the environment. It is estimated that the production of clinker, a major cement component, releases into the atmosphere around 0.84 kg of CO_2 for each kilogram of clinker produced [3]. The cement industry is responsible for 6–7% of CO_2 emissions around the world owing to anthropogenic actions [4] and contributing to 5–8% of greenhouse gases [5–9]. In this scenario, researchers for alternative types of cement are increasing around the world and could be divided into two groups: (i) supplementary cementitious materials; and (ii) alkali-activated materials.

Supplementary cementitious materials (SCM) partially replace the clinker to produce sustainable cement [10–12]. These materials should be pozzolanic, that is, react with calcium hydroxide present in the hydration of clinker and form hydrated calcium silicate. The hydrated calcium silicate is the major product of cement's hydration, which is responsible for strength and material durability. Different methods are used to classify a material as pozzolanic: (i) chemical analyses [13,14]; (ii) indirect pozzolanic activity index [15,16]; and (iii) direct pozzolanic activity index such as the Chapelle test [17,18] and Luxán test [19].

Alkali-activated materials (AAMs) result from the dissolution and polycondensation in high pH media of materials rich in silicon, aluminum, and calcium contents [20]. Thus, residues and by-products from industry or agriculture, which are often landfilled, can be used as raw materials [21–23]. For this reason, the production of AAM has great potential to release less CO_2 when compared to Portland cement [24]. However, despite the AAMs are already accepted and applied for industrial production in some countries, there is still a lack of formal methods to characterize their reactivity. This is a result of the complexity of the factors involved in the synthesis of AAMs, such as the variety of chemical composition of the precursors, types of precursors, combinations of activators, the molarity of activators, and the conditions of curing [25–28].

Regarding the activators, some points are already consolidated in the literature, such as the optimal molarity ratio to produce AAMs using sodium hydroxide as an activator [29], and the role of sodium silicate in the reaction. It is known that the greater the increase of the concentration of NaOH, the faster the precursors dissolve in the medium. However, if the concentration of OH- is too high (around 12 M), the polycondensation phase might be delayed in geopolymerization reactions [30,31]. Besides that, according to Palomo et al. [32], the presence of soluble silica in the silicate contributes to cross-links between the chains formed in the reactions, which improves the properties of alkaline binders owing to a more compact structure. However, the higher concentrations of soluble silica tend to delay the reactions due to a reduction in pH and an increase in the viscosity of the mixture [33].

Regarding the reactivity of the precursors, it is known that three main factors must be observed: (i) chemical composition; (ii) surface area; and (iii) crystallinity [34]. It is known that greater reactivity is achieved through the highest silica and alumina contents, high surface area, and greater amorphous phase content. Previous works already evaluated the reactivity of some precursors used in geopolymers [35–39]. However, these works focused on only one type of precursor, and none of them assesses the reactivity of sugarcane bagasse ash. In addition, these reactivity evaluation methods use NaOH or HF for the chemical attack to dissolve the vitreous phase of the materials. Nonetheless, as mentioned before, the vitreous phase is only one of many factors that guarantee the efficient reactivity of alkaline precursors.

Therefore, this work aims to develop a method that can characterize the reactivity of the many precursors used for the production of activated alkali materials. The method created could be used to determine the viability of the precursor for the alkaline activation through tests of simple execution and interpretation.

In this method, in addition to evaluating the amorphous phases of the precursors already exhibits in the literature [35–38], pastes were produced with commonly used precursors (blast furnace slag, silica fume, and metakaolin) and NaOH and NaOH + Na_2SiO_3 as activators for structural analysis. This proposed new step was performed by FTIR test to investigate the formation of geopolymeric bonds in these pastes. The other novelty of this method is the evaluation of the reactivity of sugarcane bagasse ash (SBCA). The SBCA has already been studied as a pozzolanic material due to its chemical composition, high potential for clinker substitution, and availability [40–47]. However, the research on SCBA as a precursor for alkaline binders is incipient.

2. Materials and Methods

2.1. Materials

Blast furnace slag was supplied by Supermix company. The silica fume was supplied by Tecnosil company. The metakaolin was supplied by Metacaulim do Brasil. Sodium hydroxide (97% purity, Êxodo Científica Fina Indústria e Comércio LTDA) and sodium silicate (14.98% Na_2O, 32.85% SiO_2 and 52.17% H_2O, Sulfal Química Limitada) were used as activators. Hydrofluoric acid (37–51% concentration) was used to assess the crystalline phases in the precursors.

The SCBA was submitted to a beneficiation process to evaluate its influence on reactivity [4,48]. The ashes samples were separated into categories according to the treatment applied, namely: (i) sugarcane bagasse ash mechanically treated (SCBAM) and (ii) sugar cane bagasse ash mechanically and heat-treated (SCBAMH). Then, the SCBAM was ground in a ball mill for 2 h at 90 rpm speed with 90 steel spheres of 30 cm in diameter. The SCBAMH was calcined in a muffle oven at 700 °C for 3 h before grinding.

2.2. Methods

The chemical composition of blast furnace slag (BFS), metakaolin (MK), silica fume (SF), and sugarcane bagasse ashes (SCBAM and SCBAMH) were determined by X-ray fluorescence analysis (XRF) using Philips/Panalytical spectrometer and are listed in Table 1. The particle size distribution in the material was measured through laser granulometry, using a Cilas 1090 Laser Particle Size Analyzer and the results are shown in Table 1.

Table 1. Chemical composition by XRF (wt%).

	BFS	**SF**	**MK**	**SCBAM**	**SCBAMH**
SiO_2	32.05	95.94	62.00	32.89	73.53
Al_2O_3	14.33	0.21	30.55	11.72	10.65
Fe_2O_3	1.27	0.12	2.51	18.26	6.14
CaO	39.46	0.35	0.04	2.90	2.39
MgO	8.77	0.41	0.25	2.82	1.39
TiO_2	0.53	0.01	1.45	5.90	0.95
K_2O	0.17	0.4	0.49	2.84	2.22
MnO	0.63	0.02	0.01	0.25	0.13
P_2O_5	<0.01	<0.01	<0.01	0.93	1.14
ZrO_2	-	<0.01	0.06	0.04	0.04
SO_3	1.43	<0.01	-	<0.01	0.02
Na_2O	0.96	<0.1	<0.1	<0.1	<0.1
Cr_2O_3	0.11	<0.01	0.02	0.27	0.20
Sum of pozzolanic oxides	47.65	96.27	95.06	62.87	90.32
Loss on ignition (LOI)	0.18	2.15	2.44	20.68	0.98
SiO_2/Al_2O_3	3.80	776.66	3.45	4.77	11.74
	Particle size distribution				
D_M (µm)	22.92	21.91	22.79	17.27	17.77
D_{10} (µm)	1.75	5.12	3.08	2.56	2.20
D_{50} (µm)	15.78	20.52	19.64	13.34	12.73
D_{90} (µm)	55.10	40.86	46.84	38.26	41.68

The BFS shows CaO as the major compound owing to its process of production [49]. SF is a by-product of silicon and ferrosilicon alloy production industries and presents silica in the range of 85–95% [50]. MK exhibits SiO_2 and Al_2O_3 as their major compounds [51]. Regarding the ashes, the SCBAM and SCBAMH are composed mainly of SiO_2, Al_2O_3, and Fe_2O_3. The heat treatment leads to an increase in SiO_2 and a decrease in Fe_2O_3 content. This behavior has been reported before [4,40].

SiO_2 and Al_2O_3 are essential oxides for the alkaline activation of low calcium precursors. At the same time, CaO and SiO_2 are the main oxides for alkaline activation of high calcium precursors. According to previous studies [34,37,52,53]. SiO_2/Al_2O_3 reactivity is fundamental for the reaction degree, the composition and structure of the N-A-S-H gel formed, and consequently the strength and durability of the low-calcium binder. Recent studies have been using this ratio from 2 to 4 to assess the reactivity of precursors [54–59]. In addition, precursors with high calcium content must have a CaO/SiO_2 ratio between 0.9 and 1.2 for efficient activation [60–64]. Considering this range, only BFS and MK would be considered appropriate precursors for alkaline activation.

Regarding the particle size test, all of the samples presented a particle size smaller than 0.5 mm which significantly increases the performance of AAMs [65]. In addition, the ashes had the smallest D_M among the materials studied, and it could be indicative of high reactivity since smaller particle size is related to higher surface area inducing higher reactivity in the material [66–68].

Materials crystal phases and mineralogical composition were analyzed by XRD. The X-ray diffraction was performed with a Shimadzu XRD-7000 diffractometer operating with Cu K-alpha radiation (40 kV/30 mA), with 2θ from 5° to 100° at a step of 2°/min. The peaks were identified using the software Match! 3 (Version 3.7.0.124) with the Crystallography Open Database (COD) revision no. 211633. The XRD patterns of SF, BFS, MK, SCBAM and SCBAMH are shown in Figure 1. BFS (Figure 1e) and SF (Figure 1c) presented a wide hump at around 30° and 23° [69], respectively, which is related to the presence of amorphous phases. In the BFS (Figure 1e), the hump is also attributed to calcium silicate oxide; and it can be attributed to the SiO_2/Al_2O_3 ratio up to 2.2 [70]. This amorphous feature present in BFS and SF is related to the reactivity in those materials. At the same time, the MK spectra (Figure 1b) exhibit intense peaks of quartz (COD 96-101-1160) that imply high silica content [51]. In addition, kaolinite (COD 96-900-9235) and muscovite (COD 96-900-6330) is also observed in MK diffraction. This high content of crystalline phases could indicate a reduction in its reactivity. The diffraction of SCBAM (Figure 1d) exhibits an angle between 10° and 35° (2θ) [41,71]. Those angles are related to silica in three forms: (i) crystalline quartz; (ii) cristobalite; and (iii) amorphous silica [43,72]. On the other hand, the amorphous hump could also be related to the presence of carbon content. The cristobalite phase in SCBAM describes the phase changing of amorphous silica during uncontrolled burning while the quartz phase is associated with the sand attached to the SCBA during harvesting [42,73]. Besides that, the amorphous content of SCBAMH (Figure 1a) decreased [40], while the quartz peak intensity increased with increasing temperature.

The analysis of the particle morphology of each material was performed using SEM and is presented in Figure 2. The scanning electron microscopy was performed on a Hitachi TM3000 scanning electron microscope under a low vacuum with a backscattered electron detector and electron acceleration voltage of 15 kV.

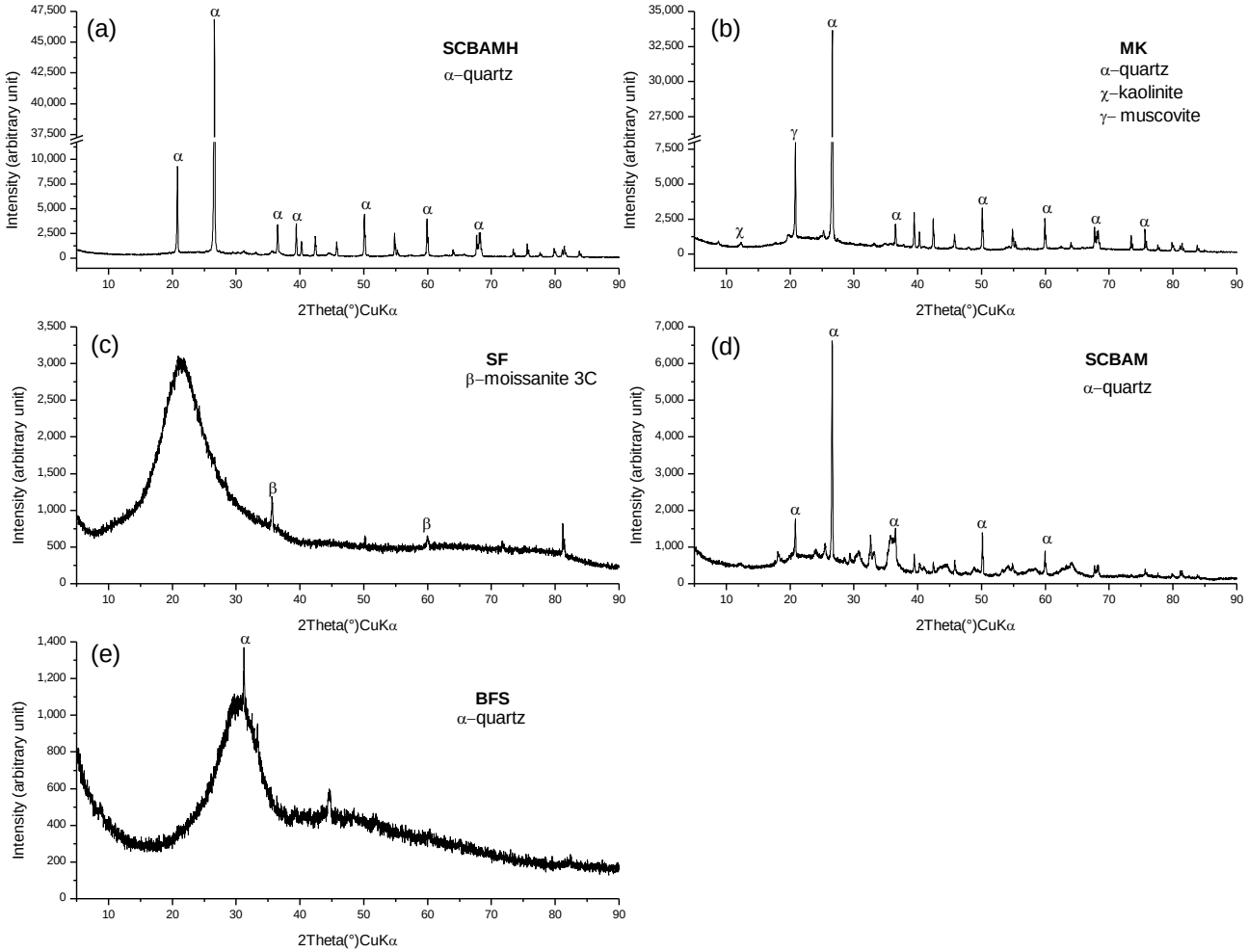
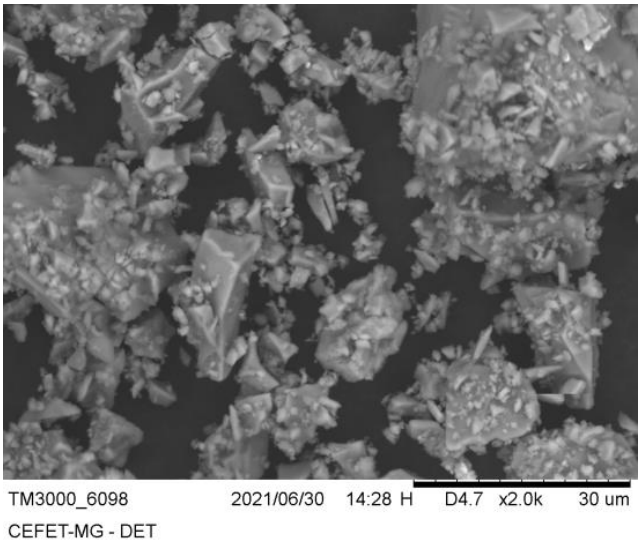
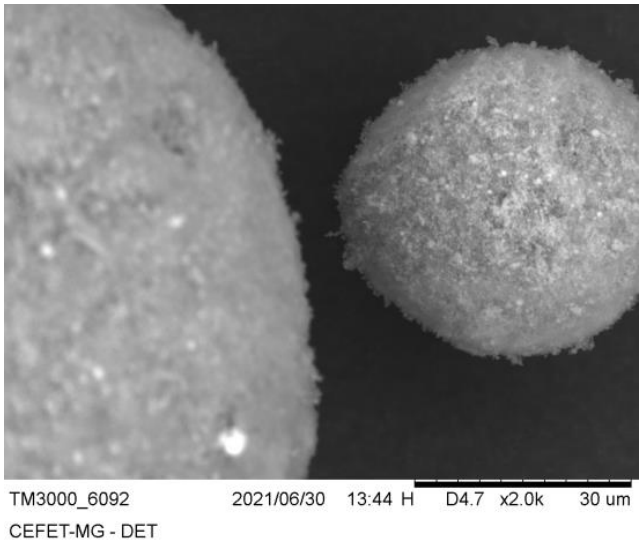


Figure 1. XDR spectrum of (**a**) SCBAMH, (**b**) MK, (**c**) SF, (**d**) SCBAM, and (**e**) BFS.

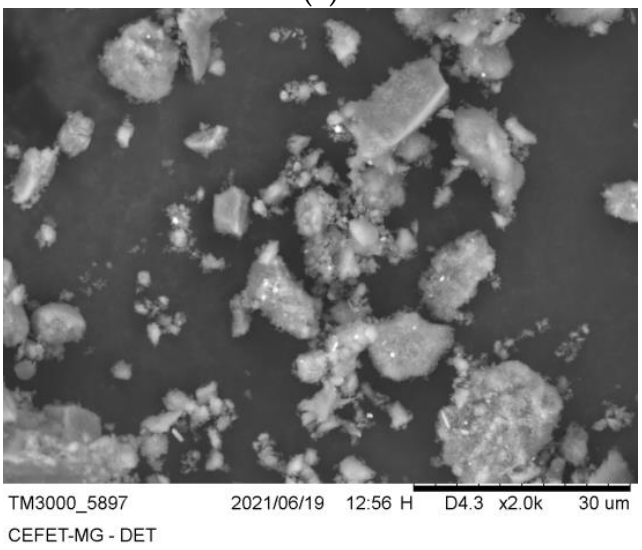
The BFS micrograph (Figure 2a) shows that the slag particles are granular and with sharp edges. BFS also exhibits a diversity of particle size and shape; the smaller particles cover the surface of the larger ones. In addition, the material has a compact appearance [74]. At the same time, the SF micrograph (Figure 2b) shows that the shape of the silica particle is spherical and can form clusters when stacked together [51]. In the MK micrograph (Figure 2c), the particles presented a granular structure; and it is possible to observe that the smallest particles agglomerate on top of larger ones. The presence of unreacted fiber is evident in the micrograph of SCBAM (Figure 2d). These fibers represent unburned material consisting basically of carbon, which does not contribute to the geopolymerization reactions. In addition, the presence of particles with different shapes can also be noticed. Spherical particles are mainly associated with Si and O and some other minor components such as MgO and Al_2O_3. Compacted and prismatic particles could also be associated with the presence of Si and O elements [75]. The presence of powdery material over the surface of the particles is also observed. As expected, there is no presence of fibers in the SCBAMH micrographs (Figure 2e). This indicates that the thermal activation could eliminate the unburned residue. The reduction of the particles could also be observed due to mechanical activation. The remaining particles are compacted and covered with a finer material on their surface.



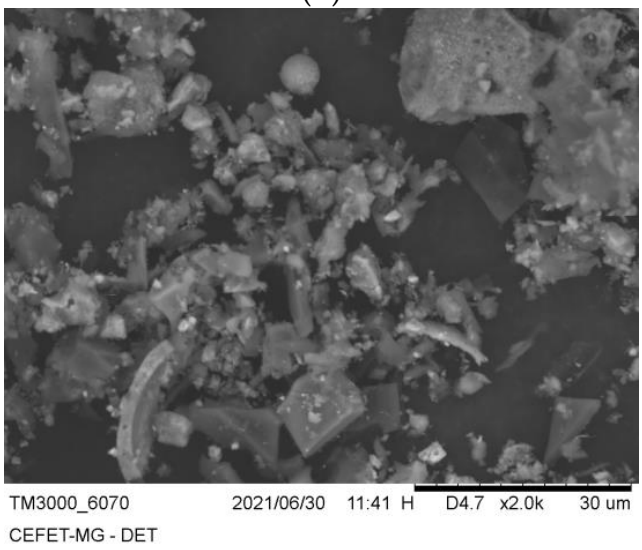
(**a**)



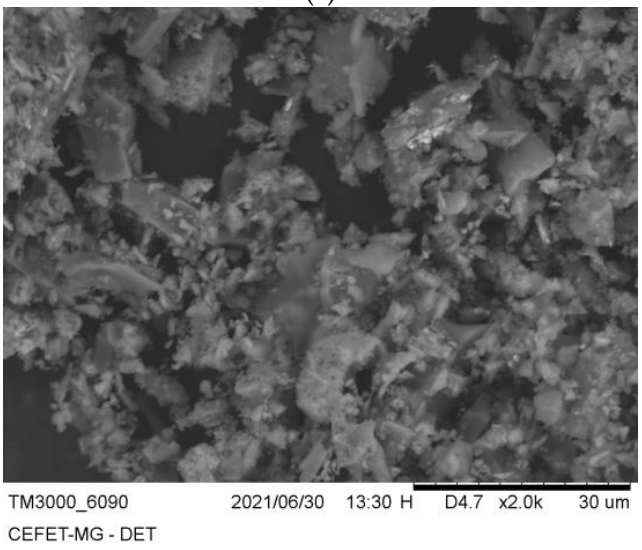
(**b**)



(**c**)



(**d**)



(**e**)

Figure 2. Micrographs of (**a**) BFS, (**b**) SF, (**c**) MK, (**d**) SCBAM, and (**e**) SCBAMH.

2.2.1. Acid Attack—Method

After preliminary characterizations, 1 g of each material was mixed in 100 mL of 1% HF solution. The mixture was stirred for 6 h at ambient temperature. After this time, the mixture was filtered in, and the residue was rinsed with deionized water until the filter reached a pH value of 7. Subsequently, the retained material was dried for 1 h in an oven at 100 °C, and its mass was recorded. After mass measurement, part of the material was reserved for further XRD testing to determine changes in the crystalline phases of the precursors. The other part of the material was subjected to calcination by thermogravimetric analyzer equipment STA7000 series of the Hitachi brand, with the aluminum crucible, flow of nitrogen gas at 60 mL/min. The sample was exposed from 25 °C to 600 °C, with an increment rate of 40 °C/min to verify the chemical constitution of the retained material.

2.2.2. Structural Analysis—Method

Pastes with the studied precursors were produced: the pastes 01 were produced exclusively with NaOH and precursor/activator ratio = 0.7, and the pastes 02 were produced with Na_2SiO_3 (SS) and NaOH (SH) at the SS/SH = 2.5 ratio and the same precursor/activator ratio as the paste 01. The concentration of NaOH solution used in the two pastes was 8 mol/L and the molar ratios of the oxides constituting the activators are shown in Table 2. After 28 days of curing, the pastes were submitted to a FTIR test in the Shimadzu IR-Prestige 21 equipment for structural analysis.

Table 2. Pastes compositions.

Precursor (g)	Paste 01	Paste 02	
	H_2O/Na_2O	H_2O/Na_2O	SiO_2/Na_2O
30	10.44	11.38	1.36

3. Results

3.1. Acid Attack—Results

The analysis of materials' mineralogical composition before and after the acid bath (Figure 3) were performed by software Match! 3 with the Crystallography Open Database (COD) revision no. 211633. According to Figure 3, the vitreous phases of precursors decrease after the acid bath. This occurs since the acid attacks these phases. The sugarcane ashes present a larger decrease of vitreous phases, which could indicate that sugarcane ashes have a high content of vitreous phases. Besides ashes, MK presents a significant decrease of theses phases. The crystallinity of SF and BFS did not change significantly. This suggests that in materials that exhibit a higher vitreous phase, the acid attack reduces the intensity of amorphous halos and maintains the material's low crystallinity degree, as can be seen in Figure 3a,b.

With regards to peaks intensity, as can be seen also at Figure 3, the intensity of all peaks usually decreases after the acid bath. However, SCBAM exhibits higher peaks after 1% HF solution. This could be associated with a reduction of vitreous phases which leads to an increase in peak intensity. Other precursors presented a reduction of the intensity of both crystalline phases and vitreous phases.

Regarding the mineralogical composition of precursors, no intense variation was observed after the acid bath, as expected for BFS and SF. The peaks of diffractograms were identified using the software Match! 3 with the Crystallography Open Database (COD) revision no. 211633 or according to literature. The diffractogram of BFS after acid bath exhibits a peak around 45° that was attributed to aluminum calcium fluoride (COD 96-100-0301) [76]. SF shows a peak around 60° assigned to silicon fluoride after an acid attack [77]. SBCAM and SCBAMH XRD spectrum exhibit quartz (COD 96-901-3322) as the main crystalline phase before and after an acid attack. MK also exhibits the same crystalline phase, muscovite (COD 96-900-6330), and quartz, before and after the acid bath.

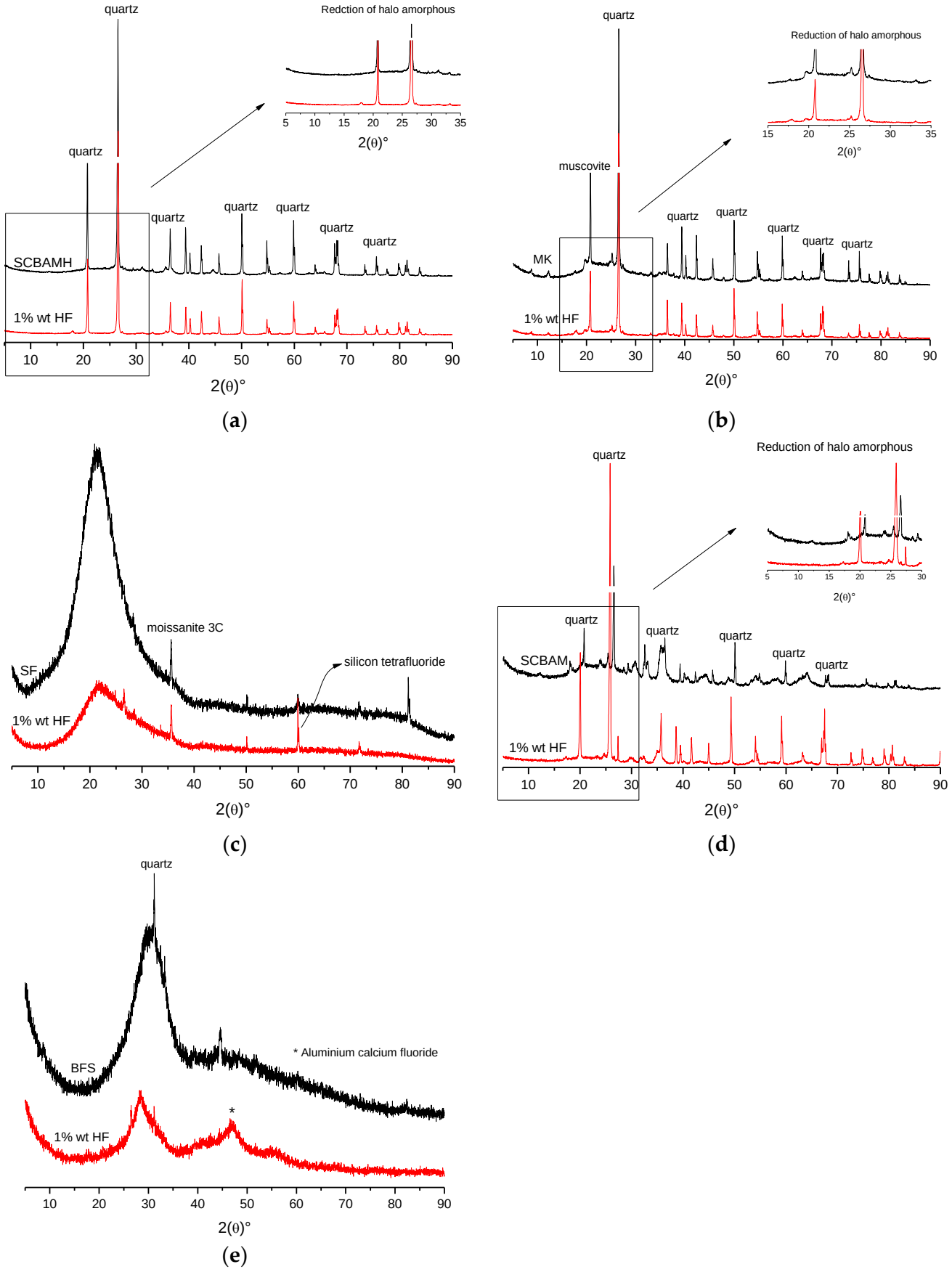


Figure 3. XRD test (**a**) SCBAMH, (**b**) MK, (**c**) SF, (**d**) SCBAM, and (**e**) BFS.

According to the thermogravimetric analysis of retained material (Figure 4a–c), SF, SCBAM, and SCBAMH exhibit similar mass loss of around 4% after an acid bath. This can be attributed to the chemical composition not changing after a 1% HF solution. Peaks of quartz exhibited on the diffraction spectrum of these materials which is a stable structure could explain this behavior [78]. SCBAM shows one stage of mass loss from 25–400 °C assigned to the removal of physically and/or chemically adsorbed water or organic matter [4,79]. SCBAMH also exhibits mass degradation until 450 °C related to free water evaporation and volatilization of organic matter. In addition, it is possible to observe a weight loss in around 500 °C attributed to the crystallization of metastable cristobalite in SCBAMH. This crystallization occurs at lower temperatures due to the metal impurities present in the ash [78,80]. SF exhibits a mass loss up to 200 °C which is associated with the release of free water, and others in the range of 400–800° that is attributed to the dehydration of the silanol groups [81].

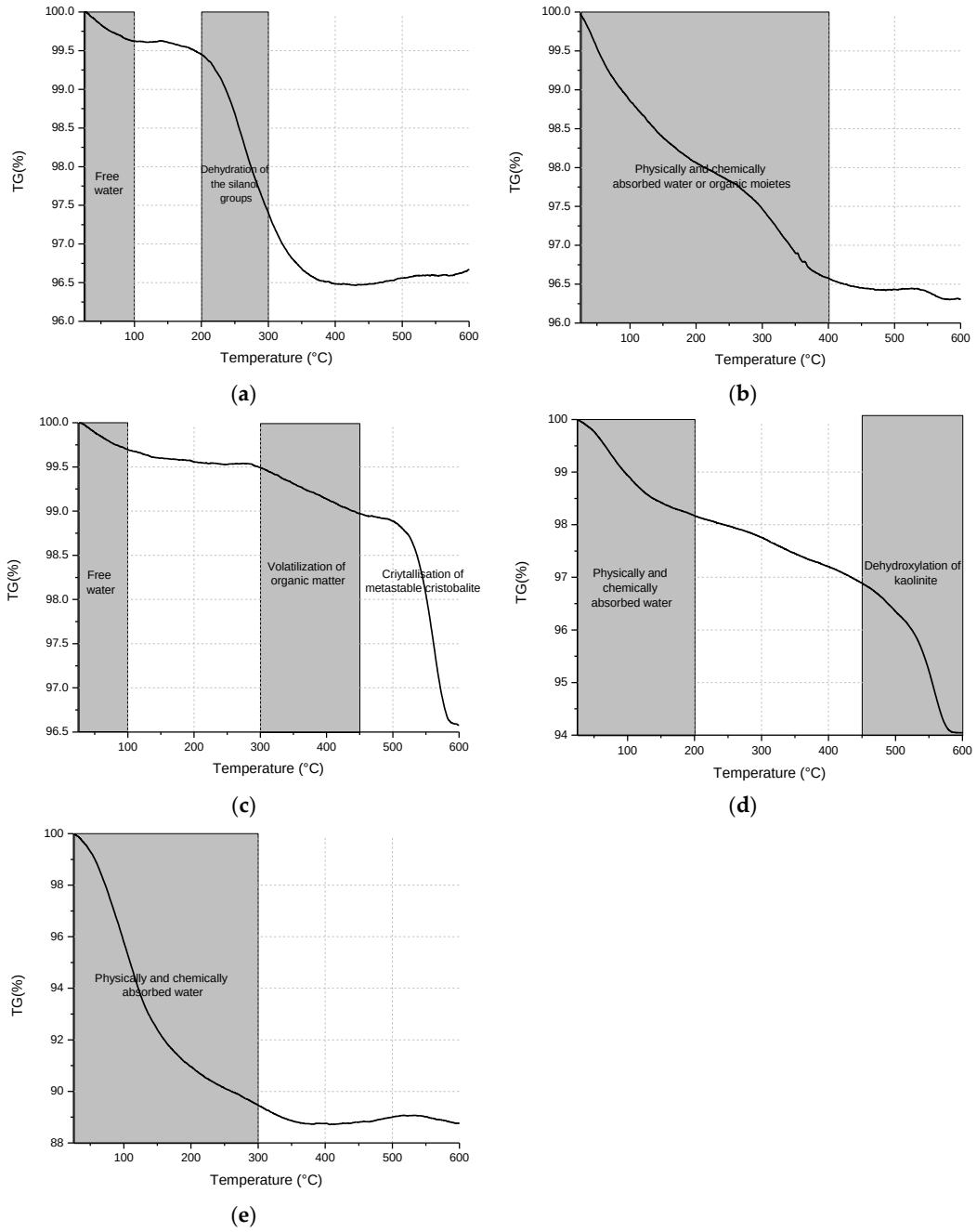


Figure 4. Thermogravimetric analysis of (**a**) SF, (**b**)SCBAM, (**c**) SCBAMH, (**d**) MK, and (**e**) BFS.

Besides that, MK also exhibits a low mass loss value at about 6% (Figure 4d). This also suggests that the presence of stable crystalline phases in these materials, such as quartz and kaolinite, reduces the mass loss degree. However, MK shows a higher loss of mass that SF, SCBAM and SCBAMH as a result of the dihydroxylation of kaolinite that occurs around 450–600 °C [82,83]. At the same time, BFS exhibits weight loss of 12% in the range of 25–300 °C, assigned to the release of physically or chemically adsorbed water. Usually, the removal of hydroxyl groups depends on their chemical bonding with metal ions. Non-coordinating hydroxyl groups or physically adsorbed water molecules are removed at a lower temperature [84].

3.2. Structural Analysis—Results

The structural analysis in pastes was carried out by FTIR test. According to Figure 5, the SF pastes did not exhibit a significant presence of hydrated products associated with O-H and OH bonds, which are attributed to bands around 3400 and 1700 cm^{-1}, respectively [85–87]. The absence of these bands could be associated with inefficient alkali activation of this precursor. In addition, there is a band at about 1500 cm^{-1} that is associated with the O-C-O bond and possible carbonation of activated samples [86,88,89]. The intensity of the characteristic Si-O-T band is reduced due to activation, and the wavenumber is shifted to lower values due to the silicon bond change through alkaline solutions addition. The Si-O bond assigned to the band around 800 cm^{-1} also reduced the intensity through activation [90]. In addition, bands at around 600 and 400 cm^{-1} associated with the Si-O-Si bond also changed [91,92]. There is a reduction of the band around 400 cm^{-1} and an appearance of the band near to 600 cm^{-1} which could indicate a structural change in the silicon bond.

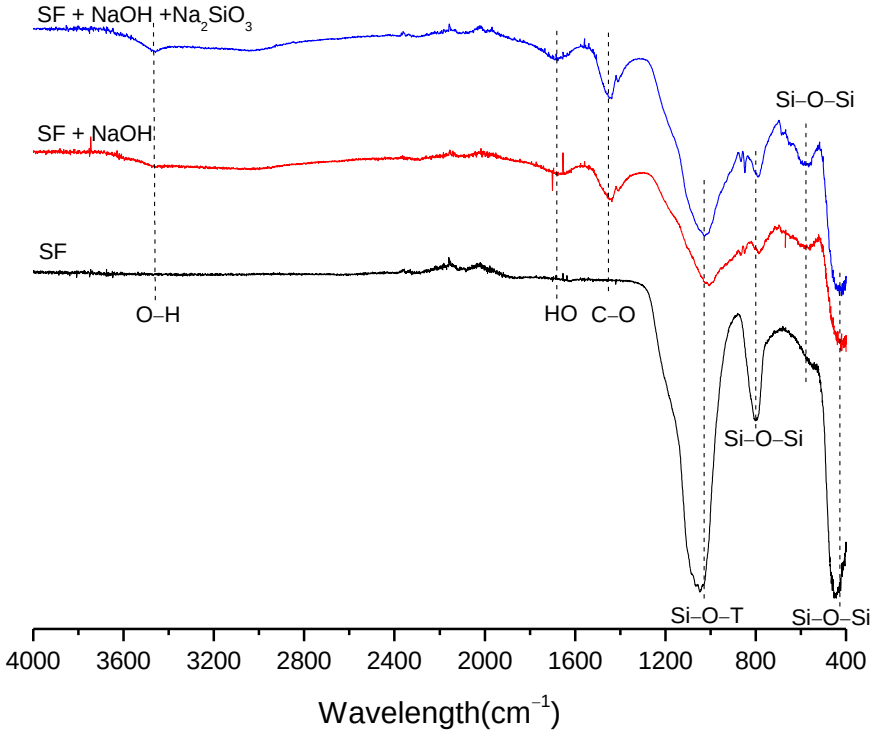


Figure 5. FTIR of SF and SF activated pastes.

FTIR spectrum of both SF activated pastes is quite similar, except for the intensity of the characteristic band of Si-O-T bond, which is more intense for the paste activated with sodium silicate and sodium hydroxide. This may be associated with the major presence of silicon oxide in this paste.

The presence of hydrated products is related to the presence of O-H bond at around 3400 cm^{-1} in activated pastes, as observed for MK-pastes (Figure 6). In addition, there is the presence of OH bond assigned to the band around 1700 cm^{-1} in these pastes which is also associated with the formation of hydrated products. The intensity of these bands could be attributed to the effective activation of the precursor. In addition, there is also the presence of the Si-O-T bond in activated pastes, and it shifted to lower values in the precursor. This change in wavenumber is attributed to the introduction of aluminum on silicon bond for N-A-S-H formation which is a characteristic product of polymerization of low calcium precursor [93,94].

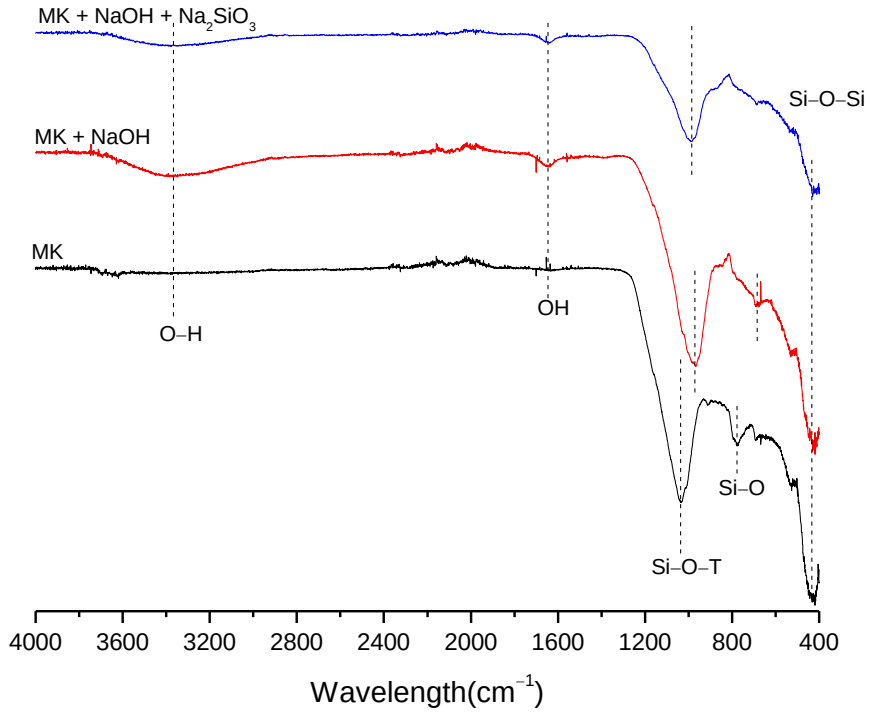


Figure 6. MK and MK activated pastes.

The band assigned to the Si-O bond, which is larger in the precursor, is attributed to 800 cm^{-1} wavenumber and exhibits a reduction of its intensity through alkaline activation. This change occurs due to the dissolution of precursors and the reorganization of silicon bonds. In addition, there is a reduction of the band near 400 cm^{-1} associated with the Si-O-Si bond which could indicate structural changes in the silicon bond.

FTIR spectrum of MK activated pastes is quite similar, except by intensity and wavenumber of a characteristic band of Si-O-T bond. The band is stronger for sodium hydroxide activation and exhibits lower values for sodium silicate activated paste. The lower wavenumber value is associated with the aluminum presence in paste structure which favors the formation of many crosslink bonds on products resulting from geopolymerization.

Figure 7 shows the FTIR spectrum of SCBAM and SCBAMH activated pastes. In the SCBAMH pastes, only the paste activated with sodium hydroxide exhibits the hydrated products, however, the bands associated with these products are not significant. In addition, the bands assigned to C-O-C, Si-O-T, Si-O, and Si-O-Si bonds exhibit similar behavior to MK. However, at the FTIR spectrum of the pure precursor, it is possible to observe a band around 700 cm^{-1} associated with the Al-O bond which decreases the intensity after activation due to the precursor dissolution [95,96].

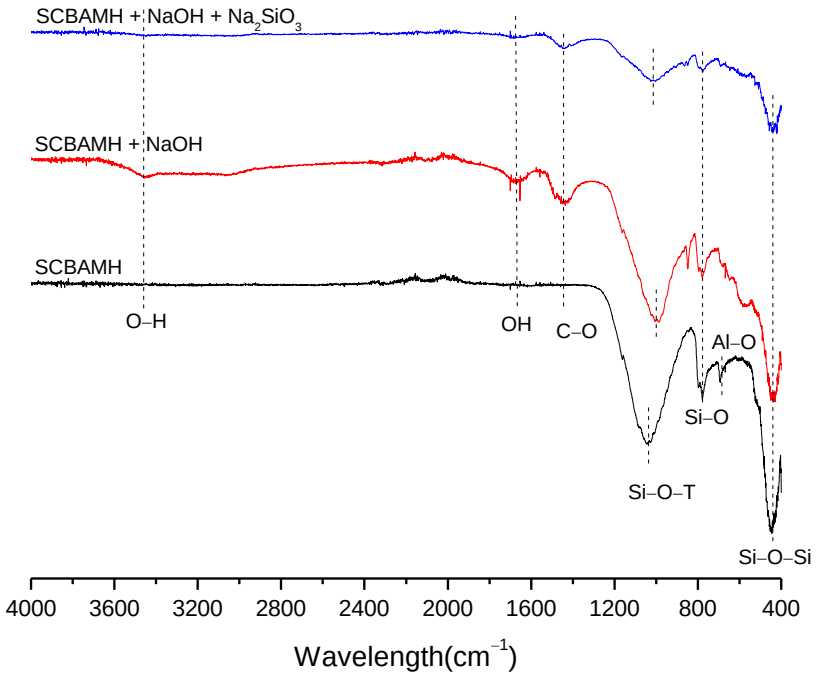


Figure 7. SCBAMH and SCBAMH activated pastes.

The absorption band for BFS-pastes (Figure 8) also exhibits similar behavior to MK-pastes. However, the characteristic band assigned to the Si-O-T bond exhibits a typical shoulder of C-(N)-A-S-H product resulting from high calcium precursor activation. It is also worth noting that the bands are stronger on BFS activation and there is a band at about 1500 cm^{-1} associated with O-C-O bonds and possible carbonation of activated samples. Another difference between the precursors is the absence of the band around 800 cm^{-1} assigned to the Si-O bond, and the presence of the band around 700 cm^{-1} associated with the Al-O bond in the precursor which becomes lower in the alkaline activation. This change occurs as a result of precursor dissolution and reorganization from aluminum bonds.

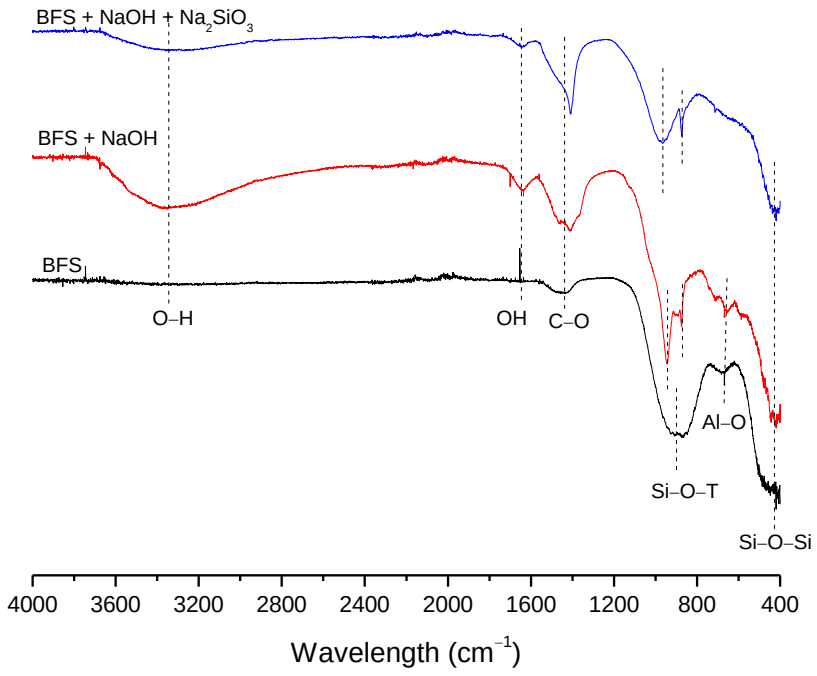


Figure 8. BFS and BFS activated pastes.

SCBAM-pastes (Figure 9) exhibits the bands assigned to hydrated products for both types of activators. The bands assigned to C-O-C, Si-O-T, Si-O, and Si-O-Si bonds exhibit similar behavior to MK. However, the characteristic band around 800 cm^{-1} associated with the Si-O bond exhibits an increase of intensity through activation, which is only observed for SCBAM-pastes. This band could be assigned to the formation of N-A-S-H in the paste samples. The presence of the band related to hydrated products could indicate that alkaline activation is effective for SCBAM.

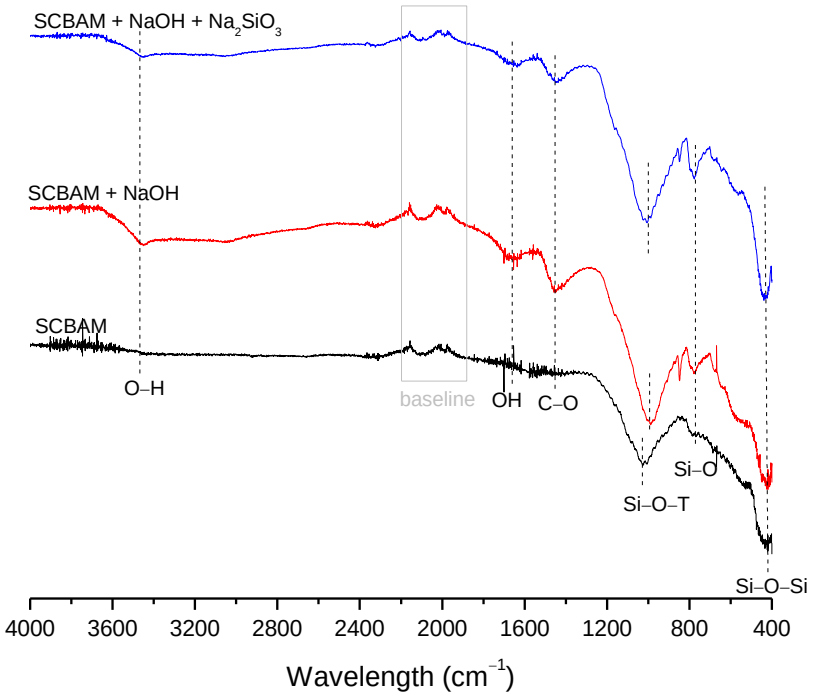


Figure 9. SCBAM and SCBAM activated pastes.

Table 3 summarizes the wavenumber of the most important bands analyzed in the present work. According to the FTIR spectra (Figures 5–9), a change in wavenumber may have occurred due to a structural change in precursors due to alkaline activation. However, there is no significant change for SCBAMH and SF, which indicates that alkaline activation was not effective for these precursors.

Table 3. Summary of bands in the FTIR spectrum.

Wavenumber (cm^{-1})	Function Band	Reference
3400	O-H	[85–87]
1700	OH	[85–87]
1500	C-O	[86,88,89]
1000	Si-O-T (T = Si or Al)	[93,94]
900	Si-O-T (T = Si or Al)	[93,94]
800	Al-O and Si-O	[90]
600	Al-O and Si-O	[95,96]
500	Si-O-Al and Si-O-Si	[91,92]

Although SF shows a higher vitreous phase and smaller particle size, the alkaline activation was not effective due to the absence of aluminum in its chemical composition. The aluminum presence is essential for N-A-S-H formation on low calcium precursors. SCBAMH also exhibits lower aluminum content (SiO_2/Al_2O_3 = 11.74), and higher crystallinity which also impairs its activation. Whereas, SCBAM shows chemical composition (SiO_2/Al_2O_3 = 4.77), significant amorphous halo, and particle size (D_M 17.27 µm) suitable for alkali activation, despite its high loss on ignition. Therefore, SCBAM is a viable

precursor for effective alkali activation. MK and BFS are already classic precursors for alkali activation and meet all requirements. According to stages proposed, two parameters could be attributed to effective alkali-activation: (i) significant amorphous halo and (ii) SiO_2/Al_2O_3 proportion from 2 to 5.

4. Discussion

Lancellotti et al. [38] studied the reactivity of bottom ash. After a chemical attack with 100 mL of 8 mol/L NaOH solution and stirred constantly for 5 h in a flask bathed at 80 °C, it concluded that the ashes were not adequate to obtain a geopolymer since its Si/Al mass ratio were below the value of 3. Kuenzel et al. [36] studied the reactivity of metakaolin through 1% (mass) HF solution for 20 h at ambient temperature and concluded that HF removes the amorphous phase in MK associated with the intensity background between 20 and 30 degrees 2θ, with the remaining sample consisting of crystalline phases present as impurities and the Si/Al mass ratio after acid attacks is equal to 2.85. Fernández-Jimenez et al. [37] studied the reactivity of fly ashes through 100 mL of 1% HF stirred for 6 h at ambient temperature and concluded that when the ashes are treated with 1% HF, most of the halo associated with its glassy constituent disappears. At the same time, these diffractograms evidence an increase in the intensity of the peaks associated with the crystalline phases. The precursors evaluated in this studied (SF, MK, BFS, SCBAM and SCBAMH) exhibits the same behavior of work of Fernández-Jimenez et al. [37].

Regarding the effect of reactivity of precursors in the mechanical and durability properties of the resulting products, previous studies concluded that the reactivity of precursors is an important parameter to a good performance of geopolymer. The higher reactivity of precursors led to a higher geopolymerization rate resulting in development of a dense and strong matrix explaining the high mechanical and durability performances [97]. At the same time, the surface area was not a fundamental parameter for determining the reactivity of the precursors in this work, since all precursors have reduced particle size. However, previous works [22,98–100] concluded that the finer particles of the precursors exhibit a faster geopolymerization and result in more formation of activation products, when there is a higher difference in particle size between the precursors.

5. Conclusions

Non-complex execution and easy-interpretation tests were proposed to help in the preliminary characterization of the reactivity of SCBA, BFS, MK, and SF as precursors for alkali-activated materials. According to these tests, the following conclusions can be drawn:

- The surface area is not relevant when the materials exhibit particles size medium smaller than 23 μm.
- The amorphous area is only relevant if the material exhibits the optimal chemical composition.
- The chemical composition is a crucial parameter of alkali activation.
- Potential precursors for effective alkali activation should exhibit significant amorphous halo and SiO_2/Al_2O_3 proportion from 2 to 5.
- Silica fume is not viable as a single-precursor for alkali-activation due to the absence of aluminum on its chemical composition.
- Sugarcane bagasse ash mechanically and heat-treated is not a suitable precursor for alkali-activation due to its crystalline character and lower aluminum content.
- Sugarcane bagasse ash mechanically-treated, blast furnace slag, and metakaolin are viable precursors for alkali-activation.

Future research on determining the maximum acceptable crystallinity for viable precursors is highly recommended.

Author Contributions: Conceptualization, S.F. and A.C.d.S.B.; Methodology, S.F. and A.C.d.S.B.; Software, M.V.d.M.S.S.; Validation, A.C.d.S.B.; Formal Analysis, S.F. and A.C.d.S.B.; Investigation, S.F.; Resources, A.C.d.S.B., M.V.d.M.S.S. and P.H.R.B.; Data Curation, S.F.; Writing—S.F. and L.N.S.; Writing—Review & Edit, S.F., L.N.S. and A.C.d.S.B.; Visualization, S.F. and A.C.d.S.B.; Supervision, A.C.d.S.B. and P.H.R.B.; Project Administration, A.C.d.S.B., M.V.d.M.S.S. and P.H.R.B.; Funding Acquisition, A.C.d.S.B., M.V.d.M.S.S. and P.H.R.B. All authors have read and agreed to the published version of the manuscript.

Funding: This work was supported by Energy Company of Minas Gerais (CEMIG) and the National Electric Energy Agency (ANEEL) for funding through the PD ANEEL CEMIG GT616 project, the Minas Gerais State Research Foundation (FAPEMIG) [grant number APQ-01425-22], and National Council for Scientific and Technological Development (CNPq) [grant number PQ 315653/2020-5].

Data Availability Statement: The data presented in this study are available on request from the corresponding author.

Acknowledgments: The authors would like to thank Energy Company of Minas Gerais (CEMIG) and the National Electric Energy Agency (ANEEL) for funding through the PD ANEEL CEMIG GT616 project. The Minas Gerais Research Support Foundation (FAPEMIG) for their assistance with the infrastructure and National Council for Scientific and Technological Development (CNPq) for the research productivity incentive grant.

Conflicts of Interest: The authors declare no competing financial interest or personal relationship that could appear to influence the work reported in this paper.

References

1. WBCSD. *Guidelines for Co-Processing Fuels and Raw Materials in Cement Manufacturing*; World Business Council for Sustainable Development: Geneva, Switzerland, 2014.
2. United Nations. *World Population Prospects 2019*; United Nations: New York, NY, USA, 2019.
3. Sanjuán, M.Á.; Andrade, C.; Mora, P.; Zaragoza, A. Carbon Dioxide Uptake by Cement-Based Materials: A Spanish Case Study. *Appl. Sci.* **2020**, *10*, 339. [CrossRef]
4. Yadav, A.L.; Sairam, V.; Srinivasan, K.; Muruganandam, L. Synthesis and characterization of geopolymer from metakaolin and sugarcane bagasse ash. *Constr. Build. Mater.* **2020**, *258*, 119231. [CrossRef]
5. Gunasekara, C.; Law, D.W.; Setunge, S.; Sanjayan, J.G. Zeta potential, gel formation and compressive strength of low calcium fly ash geopolymers. *Constr. Build. Mater.* **2015**, *95*, 592–599. [CrossRef]
6. Srividhya, S.; Vidjeapriya, R.; Neelamegam, M. Enhancing the performance of hyposludge concrete beams using basalt fiber and latex under cyclic loading. *Comput. Concr.* **2021**, *28*, 93–105. [CrossRef]
7. Prakash, R.; Thenmozhi, R.; Raman, S.N.; Subramanian, C.; Divyah, N. An investigation of key mechanical and durability properties of coconut shell concrete with partial replacement of fly ash. *Struct. Concr.* **2021**, *22*, E985–E996. [CrossRef]
8. Prakash, R.; Raman, S.N.; Subramanian, C.; Divyah, N. Eco-friendly fiber-reinforced concretes. In *Handbook of Sustainable Concrete and Industrial Waste Management*; Elsevier: Amsterdam, The Netherlands, 2022; pp. 109–145.
9. Prakash, R.; Thenmozhi, R.; Raman, S.N.; Subramanian, C.; Divyah, N. Mechanical characterisation of sustainable fibre-reinforced lightweight concrete incorporating waste coconut shell as coarse aggregate and sisal fibre. *Int. J. Environ. Sci. Technol.* **2021**, *18*, 1579–1590. [CrossRef]
10. Scrivener, K.L.; John, V.M.; Gartner, E.M. Eco-efficient cements: Potential economically viable solutions for a low-CO2 cement-based materials industry. *Cem. Concr. Res.* **2018**, *114*, 2–26. [CrossRef]
11. Prakash, R.; Thenmozhi, R.; Raman, S.N.; Subramanian, C. Characterization of eco-friendly steel fiber-reinforced concrete containing waste coconut shell as coarse aggregates and fly ash as partial cement replacement. *Struct. Concr.* **2020**, *21*, 437–447. [CrossRef]
12. Prakash, R.; Raman, S.N.; Divyah, N.; Subramanian, C.; Vijayaprabha, C.; Praveenkumar, S. Fresh and mechanical characteristics of roselle fibre reinforced self-compacting concrete incorporating fly ash and metakaolin. *Constr. Build. Mater.* **2021**, *290*, 123209. [CrossRef]
13. *ABNT NBR 12653*; Materiais Pozolânicos—Requisitos. Associação Brasileira de Normas Técnicas (ABNT): Rio de Janeiro, Brazil, 2014.
14. *ASTM C618-19*; Specification for Coal Fly Ash and Raw or Calcined Natural Pozzolan for Use in Concrete. American Society for Testing and Materials: West Conshohocken, PA, USA, 2019.
15. *ABNT NBR 5752*; Materiais Pozolânicos—Determinação do Índice de Desempenho Com Cimento Portland Aos 28 Dias. Associação Brasileira de Normas Técnicas (ABNT): Rio de Janeiro, Brazil, 2014.

16. *ASTM C311/C311M-18*; Test Methods for Sampling and Testing Fly Ash or Natural Pozzolans for Use in Portland-Cement Concrete. American Society for Testing and Materials: West Conshohocken, PA, USA, 2018.
17. *ABNT NBR 15895*; Materiais Pozolânicos—Determinação do Teor de Hidróxido de Cálcio Fixado—Método Chapelle Modificado. Associação Brasileira de Normas Técnicas (ABNT): Rio de Janeiro, Brazil, 2010.
18. *AFNOR NF P 18-513*; Pozzolanic Addition for Concrete—Metakaolin—Definitions, Specifications and Compliance Criteria. AFNOR: Paris, France, 2012.
19. Luxán, M.P.D.; Madruga, F.; Saavedra, J. Rapid evaluation of pozzolanic activity of natural products by conductivity measurement. *Cem. Concr. Res.* **1989**, *19*, 63–68. [CrossRef]
20. Yasaswini, K.; Rao, A.V. Behaviour of geopolymer concrete at elevated temperature. *Mater. Today Proc.* **2020**, *33*, 239–244. [CrossRef]
21. Akbar, A.; Farooq, F.; Shafique, M.; Aslam, F.; Alyousef, R.; Alabduljabbar, H. Sugarcane bagasse ash-based engineered geopolymer mortar incorporating propylene fibers. *J. Build. Eng.* **2021**, *33*, 101492. [CrossRef]
22. Zhang, Y.; Xiao, R.; Jiang, X.; Li, W.; Zhu, X.; Huang, B. Effect of particle size and curing temperature on mechanical and microstructural properties of waste glass-slag-based and waste glass-fly ash-based geopolymers. *J. Clean. Prod.* **2020**, *273*, 122970. [CrossRef]
23. Zhou, S.; Ma, C.; Long, G.; Xie, Y. A novel non-Portland cementitious material: Mechanical properties, durability and characterization. *Constr. Build. Mater.* **2020**, *238*, 117671. [CrossRef]
24. Cai, J.; Li, X.; Tan, J.; Vandevyvere, B. Thermal and compressive behaviors of fly ash and metakaolin-based geopolymer. *J. Build. Eng.* **2020**, *30*, 101307. [CrossRef]
25. Zhang, Z.; Provis, J.L.; Reid, A.; Wang, H. Fly ash-based geopolymers: The relationship between composition, pore structure and efflorescence. *Cem. Concr. Res.* **2014**, *64*, 30–41. [CrossRef]
26. Longhi, M.A.; Rodríguez, E.D.; Walkley, B.; Zhang, Z.; Kirchheim, A.P. Metakaolin-based geopolymers: Relation between formulation, physicochemical properties and efflorescence formation. *Compos. Part B Eng.* **2020**, *182*, 107671. [CrossRef]
27. Longhi, M.A.; Walkley, B.; Rodríguez, E.D.; Kirchheim, A.P.; Zhang, Z.; Wang, H. New selective dissolution process to quantify reaction extent and product stability in metakaolin-based geopolymers. *Compos. Part B Eng.* **2019**, *176*, 107172. [CrossRef]
28. Zhang, Z.; Provis, J.L.; Ma, X.; Reid, A.; Wang, H. Efflorescence and subflorescence induced microstructural and mechanical evolution in fly ash-based geopolymers. *Cem. Concr. Compos.* **2018**, *92*, 165–177. [CrossRef]
29. Nmiri, A.; Duc, M.; Hamdi, N.; Yazoghli-Marzouk, O.; Srasra, E. Replacement of alkali silicate solution with silica fume in metakaolin-based geopolymers. *Int. J. Miner. Metall. Mater.* **2019**, *26*, 555–564. [CrossRef]
30. Panias, D.; Giannopoulou, I.P.; Perraki, T. Effect of synthesis parameters on the mechanical properties of fly ash-based geopolymers. *Colloids Surf. A Physicochem. Eng. Asp.* **2007**, *301*, 246–254. [CrossRef]
31. Zhang, Z.; Yao, X.; Zhu, H.; Chen, Y. Role of water in the synthesis of calcined kaolin-based geopolymer. *Appl. Clay Sci.* **2009**, *43*, 218–223. [CrossRef]
32. Palomo, A.; Fernández-Jiménez, A.; Criado, M. «Geopolimeros»: Una única base química y diferentes microestructuras. *Mater. Constr.* **2004**, *54*, 77–91. [CrossRef]
33. Duxson, P.; Provis, J.L.; Lukey, G.C.; Mallicoat, S.W.; Kriven, W.M.; van Deventer, J.S.J. Understanding the relationship between geopolymer composition, microstructure and mechanical properties. *Colloids Surf. A Physicochem. Eng. Asp.* **2005**, *269*, 47–58. [CrossRef]
34. Li, C.; Sun, H.; Li, L. A review: The comparison between alkali-activated slag (Si+Ca) and metakaolin (Si+Al) cements. *Cem. Concr. Res.* **2010**, *40*, 1341–1349. [CrossRef]
35. Ruiz-Santaquiteria, C.; Skibsted, J.; Fernández-Jiménez, A.; Palomo, A. Alkaline solution/binder ratio as a determining factor in the alkaline activation of aluminosilicates. *Cem. Concr. Res.* **2012**, *42*, 1242–1251. [CrossRef]
36. Kuenzel, C.; Neville, T.P.; Donatello, S.; Vandeperre, L.; Boccaccini, A.R.; Cheeseman, C.R. Influence of metakaolin characteristics on the mechanical properties of geopolymers. *Appl. Clay Sci.* **2013**, *83–84*, 308–314. [CrossRef]
37. Fernández-Jimenez, A.; De La Torre, A.G.; Palomo, A.; López-Olmo, G.; Alonso, M.M.; Aranda, M.A.G. Quantitative determination of phases in the alkali activation of fly ash. Part I. Potential ash reactivity. *Fuel* **2006**, *85*, 625–634. [CrossRef]
38. Lancellotti, I.; Ponzoni, C.; Barbieri, L.; Leonelli, C. Alkali activation processes for incinerator residues management. *Waste Manag.* **2013**, *33*, 1740–1749. [CrossRef]
39. Liu, J.; Doh, J.-H.; Ong, D.E.L.; Liu, Z.; Hadi, M.N.S. Methods to evaluate and quantify the geopolymerization reactivity of waste-derived aluminosilicate precursor in alkali-activated material: A state-of-the-art review. *Constr. Build. Mater.* **2023**, *362*, 129784. [CrossRef]
40. Cordeiro, G.C.; Barroso, T.R.; Toledo Filho, R.D. Enhancement the Properties of Sugar Cane Bagasse Ash with High Carbon Content by a Controlled Re-calcination Process. *KSCE J. Civ. Eng.* **2018**, *22*, 1250–1257. [CrossRef]
41. Ríos-Parada, V.; Jiménez-Quero, V.G.; Valdez-Tamez, P.L.; Montes-García, P. Characterization and use of an untreated Mexican sugarcane bagasse ash as supplementary material for the preparation of ternary concretes. *Constr. Build. Mater.* **2017**, *157*, 83–95. [CrossRef]

42. Cordeiro, G.C.C.; Tavares, L.M.M.; Toledo Filho, R.D.D. Improved pozzolanic activity of sugar cane bagasse ash by selective grinding and classification. *Cem. Concr. Res.* **2016**, *89*, 269–275. [CrossRef]
43. Bahurudeen, A.; Santhanam, M. Influence of different processing methods on the pozzolanic performance of sugarcane bagasse ash. *Cem. Concr. Compos.* **2015**, *56*, 32–45. [CrossRef]
44. Maldonado-García, M.A.; Hernández-Toledo, U.I.; Montes-García, P.; Valdez-Tamez, P.L. The influence of untreated sugarcane bagasse ash on the microstructural and mechanical properties of mortars. *Mater. Constr.* **2018**, *68*, 148. [CrossRef]
45. Arenas-Piedrahita, J.C.; Montes-García, P.; Mendoza-Rangel, J.M.; López Calvo, H.Z.; Valdez-Tamez, P.L.; Martínez-Reyes, J. Mechanical and durability properties of mortars prepared with untreated sugarcane bagasse ash and untreated fly ash. *Constr. Build. Mater.* **2016**, *105*, 69–81. [CrossRef]
46. de Soares, M.M.N.S.; Garcia, D.C.S.; Figueiredo, R.B.; Aguilar, M.T.P.; Cetlin, P.R. Comparing the pozzolanic behavior of sugar cane bagasse ash to amorphous and crystalline SiO2. *Cem. Concr. Compos.* **2016**, *71*, 20–25. [CrossRef]
47. Cordeiro, G.C.; Andreão, P.V.; Tavares, L.M. Pozzolanic properties of ultrafine sugar cane bagasse ash produced by controlled burning. *Heliyon* **2019**, *5*, e02566. [CrossRef]
48. Shcherban', E.M.; Stel'makh, S.A.; Beskopylny, A.; Mailyan, L.R.; Meskhi, B. Influence of Mechanochemical Activation of Concrete Components on the Properties of Vibro-Centrifugated Heavy Concrete. *Appl. Sci.* **2021**, *11*, 10647. [CrossRef]
49. Mancini, A.; Lothenbach, B.; Geng, G.; Grolimund, D.; Sanchez, D.F.; Fakra, S.C.; Dähn, R.; Wehrli, B.; Wieland, E. Iron speciation in blast furnace slag cements. *Cem. Concr. Res.* **2021**, *140*, 106287. [CrossRef]
50. Mehta, A.; Ashish, D.K. Silica fume and waste glass in cement concrete production: A review. *J. Build. Eng.* **2020**, *29*, 100888. [CrossRef]
51. Raheem, A.A.; Abdulwahab, R.; Kareem, M.A. Incorporation of metakaolin and nanosilica in blended cement mortar and concrete—A review. *J. Clean. Prod.* **2021**, *290*, 125852. [CrossRef]
52. Pal, S.C.; Mukherjee, A.; Pathak, S.R. Investigation of hydraulic activity of ground granulated blast furnace slag in concrete. *Cem. Concr. Res.* **2003**, *33*, 1481–1486. [CrossRef]
53. Fernández-Jiménez, A.; Palomo, A. Characterisation of fly ashes. Potential reactivity as alkaline cements. *Fuel* **2003**, *82*, 2259–2265. [CrossRef]
54. Chindaprasirt, P.; De Silva, P.; Sagoe-Crentsil, K.; Hanjitsuwan, S. Effect of SiO_2 and Al_2O_3 on the setting and hardening of high calcium fly ash-based geopolymer systems. *J. Mater. Sci.* **2012**, *47*, 4876–4883. [CrossRef]
55. Garcia-Lodeiro, I.; Fernández-Jimenez, A.; Pena, P.; Palomo, A. Alkaline activation of synthetic aluminosilicate glass. *Ceram. Int.* **2014**, *40*, 5547–5558. [CrossRef]
56. Kovalchuk, G.; Fernández-Jiménez, A.; Palomo, A. Alkali-activated fly ash. Relationship between mechanical strength gains and initial ash chemistry. *Mater. Constr.* **2008**, *58*, 35–52. [CrossRef]
57. Criado, M.; Fernández-Jiménez, A.; Palomo, A. Alkali activation of fly ash. Part III: Effect of curing conditions on reaction and its graphical description. *Fuel* **2010**, *89*, 3185–3192. [CrossRef]
58. Pimraksa, K.; Chindaprasirt, P.; Rungchet, A.; Sagoe-Crentsil, K.; Sato, T. Lightweight geopolymer made of highly porous siliceous materials with various Na_2O/Al_2O_3 and SiO_2/Al_2O_3 ratios. *Mater. Sci. Eng. A* **2011**, *528*, 6616–6623. [CrossRef]
59. Barreto, I.A.R.; Costa, M.L.D. Use of the clayey cover of bauxite deposits of the Amazon region for geopolymer synthesis and its application in red ceramics. *Constr. Build. Mater.* **2021**, *300*, 124318. [CrossRef]
60. Wang, S.D.; Scrivener, K.L. Hydration products of alkali activated slag cement. *Cem. Concr. Res.* **1995**, *25*, 561–571. [CrossRef]
61. Wang, S.D.; Pu, X.C.; Scrivener, K.L.; Pratt, P.L. Alkali-activated slag cement and concrete: A review of properties and problems. *Adv. Cem. Res.* **1995**, *7*, 93–102. [CrossRef]
62. Puertas, F.; Palacios, M.; Manzano, H.; Dolado, J.S.; Rico, A.; Rodríguez, J. A model for the C-A-S-H gel formed in alkali-activated slag cements. *J. Eur. Ceram. Soc.* **2011**, *31*, 2043–2056. [CrossRef]
63. Myers, R.J.; Bernal, S.A.; San Nicolas, R.; Provis, J.L. Generalized Structural Description of Calcium–Sodium Aluminosilicate Hydrate Gels: The Cross-Linked Substituted Tobermorite Model. *Langmuir* **2013**, *29*, 5294–5306. [CrossRef] [PubMed]
64. Fernández-Jiménez, A.; Puertas, F.; Sobrados, I.; Sanz, J. Structure of Calcium Silicate Hydrates Formed in Alkaline-Activated Slag: Influence of the Type of Alkaline Activator. *J. Am. Ceram. Soc.* **2003**, *86*, 1389–1394. [CrossRef]
65. Pommer, V.; Vejmelková, E.; Černý, R.; Keppert, M. Alkali-activated waste ceramics: Importance of precursor particle size distribution. *Ceram. Int.* **2021**, *47*, 31574–31582. [CrossRef]
66. Barbosa, W.; Ramalho, R.D.P.; Portella, K.F. Influence of gypsum fineness in the first hours of cement paste: Hydration kinetics and rheological behaviour. *Constr. Build. Mater.* **2018**, *184*, 304–310. [CrossRef]
67. Scrivener, K.; Ouzia, A.; Juilland, P.; Kunhi Mohamed, A. Advances in understanding cement hydration mechanisms. *Cem. Concr. Res.* **2019**, *124*, 105823. [CrossRef]
68. Nath, S.K.; Kumar, S. Role of particle fineness on engineering properties and microstructure of fly ash derived geopolymer. *Constr. Build. Mater.* **2020**, *233*, 117294. [CrossRef]
69. Yaseri, S.; Hajiaghaei, G.; Mohammadi, F.; Mahdikhani, M.; Farokhzad, R. The role of synthesis parameters on the workability, setting and strength properties of binary binder based geopolymer paste. *Constr. Build. Mater.* **2017**, *157*, 534–545. [CrossRef]

70. Yao, Y.; Wang, Y.; Wei, Q.; Cui, S.; Hao, L. Effect of the Formation of Amorphous Networks on the Structure and Hydration Characteristics of Granulated Blast Furnace Slag. *Materials* **2020**, *13*, 1462. [CrossRef]
71. Setayesh Gar, P.; Suresh, N.; Bindiganavile, V. Sugar cane bagasse ash as a pozzolanic admixture in concrete for resistance to sustained elevated temperatures. *Constr. Build. Mater.* **2017**, *153*, 929–936. [CrossRef]
72. Cordeiro, G.C.; Kurtis, K.E. Effect of mechanical processing on sugar cane bagasse ash pozzolanicity. *Cem. Concr. Res.* **2017**, *97*, 41–49. [CrossRef]
73. Cordeiro, G.C.; Toledo Filho, R.D.; Tavares, L.M.; Fairbairn, E.M.R. Pozzolanic activity and filler effect of sugar cane bagasse ash in Portland cement and lime mortars. *Cem. Concr. Compos.* **2008**, *30*, 410–418. [CrossRef]
74. Yildirim, I.Z.; Prezzi, M. Chemical, mineralogical, and morphological properties of steel slag. *Adv. Civ. Eng.* **2011**, *2011*, 463638. [CrossRef]
75. Tchakouté, H.K.; Rüscher, C.H.; Hinsch, M.; Djobo, J.N.Y.; Kamseu, E.; Leonelli, C. Utilization of sodium waterglass from sugar cane bagasse ash as a new alternative hardener for producing metakaolin-based geopolymer cement. *Geochemistry* **2017**, *77*, 257–266. [CrossRef]
76. García-Delgado, C.; Cala, V.; Eymar, E. Influence of chemical and mineralogical properties of organic amendments on the selection of an adequate analytical procedure for trace elements determination. *Talanta* **2012**, *88*, 375–384. [CrossRef]
77. Zhou, F.; Hu, B.; Cui, B.; Liu, F.; Liu, F.; Wang, W.; Liu, Y.; Lu, R.; Hu, Y.-M.; Zhang, Y.; et al. Preparation and Characteristics of Polyaluminium Chloride by Utilizing Fluorine-Containing Waste Acidic Mother Liquid from Clay-Brine Synthetic Cryolite Process. *J. Chem.* **2014**, *2014*, 274126. [CrossRef]
78. Milonjić, S.K.; Čerović, L.S.; Čokeša, D.M.; Zec, S. The influence of cationic impurities in silica on its crystallization and point of zero charge. *J. Colloid Interface Sci.* **2007**, *309*, 155–159. [CrossRef]
79. Castaldelli, V.N.; Akasaki, J.L.; Melges, J.L.P.; Tashima, M.M.; Soriano, L.; Borrachero, M.V.; Monzó, J.; Payá, J.; Castaldelli, V.N.; Monzó, J.; et al. Use of Slag/Sugar Cane Bagasse Ash (SCBA) Blends in the Production of Alkali-Activated Materials. *Materials* **2013**, *6*, 3108–3127. [CrossRef] [PubMed]
80. Kolawole, J.T.; Babafemi, A.J.; Fanijo, E.; Chandra Paul, S.; Combrinck, R. State-of-the-art review on the use of sugarcane bagasse ash in cementitious materials. *Cem. Concr. Compos.* **2021**, *118*, 103975. [CrossRef]
81. Sarawade, P.B.; Kim, J.-K.; Hilonga, A.; Kim, H.T. Recovery of high surface area mesoporous silica from waste hexafluorosilicic acid (H_2SiF_6) of fertilizer industry. *J. Hazard. Mater.* **2010**, *173*, 576–580. [CrossRef] [PubMed]
82. Rashad, A.M. Metakaolin as cementitious material: History, scours, production and composition—A comprehensive overview. *Constr. Build. Mater.* **2013**, *41*, 303–318. [CrossRef]
83. Irfan Khan, M.; Khan, H.U.; Azizli, K.; Sufian, S.; Man, Z.; Siyal, A.A.; Muhammad, N.; Faiz ur Rehman, M. The pyrolysis kinetics of the conversion of Malaysian kaolin to metakaolin. *Appl. Clay Sci.* **2017**, *146*, 152–161. [CrossRef]
84. Ansari, A.A.; Parchur, A.K.; Labis, J.P.; Shar, M.A.; Khan, A. Highly hydrophilic CaF_2:Yb/Er upconversion nanoparticles: Structural, morphological, and optical properties. *J. Fluor. Chem.* **2021**, *247*, 109820. [CrossRef]
85. Sun, Z.; Vollpracht, A. One year geopolymerisation of sodium silicate activated fly ash and metakaolin geopolymers. *Cem. Concr. Compos.* **2019**, *95*, 98–110. [CrossRef]
86. Ismail, I.; Bernal, S.A.; Provis, J.L.; San Nicolas, R.; Hamdan, S.; van Deventer, J.S.J. Modification of phase evolution in alkali-activated blast furnace slag by the incorporation of fly ash. *Cem. Concr. Compos.* **2014**, *45*, 125–135. [CrossRef]
87. Wang, Y.; Cao, Y.; Zhang, Z.; Huang, J.; Zhang, P.; Ma, Y.; Wang, H. Study of acidic degradation of alkali-activated materials using synthetic C-(N)-A-S-H and N-A-S-H gels. *Compos. Part B Eng.* **2022**, *230*, 109510. [CrossRef]
88. Jain, B.; Sancheti, G.; Jain, V. FTIR analysis of silica fume and iron dust added concrete. *Mater. Today Proc.* **2022**, *60*, 777–781. [CrossRef]
89. Reig, F. FTIR quantitative analysis of calcium carbonate (calcite) and silica (quartz) mixtures using the constant ratio method. Application to geological samples. *Talanta* **2002**, *58*, 811–821. [CrossRef]
90. Wang, Y.; Zhao, J. Comparative study on flame retardancy of silica fume-based geopolymer activated by different activators. *J. Alloys Compd.* **2018**, *743*, 108–114. [CrossRef]
91. Kapeluszna, E.; Kotwica, Ł.; Różycka, A.; Gołek, Ł. Incorporation of Al in C-A-S-H gels with various Ca/Si and Al/Si ratio: Microstructural and structural characteristics with DTA/TG, XRD, FTIR and TEM analysis. *Constr. Build. Mater.* **2017**, *155*, 643–653. [CrossRef]
92. Tchakoute Kouamo, H.; Elimbi, A.; Mbey, J.A.A.; Ngally Sabouang, C.J.J.; Njopwouo, D. The effect of adding alumina-oxide to metakaolin and volcanic ash on geopolymer products: A comparative study. *Constr. Build. Mater.* **2012**, *35*, 960–969. [CrossRef]
93. Nasab, G.M.; Golestanifard, F.; MacKenzie, K.J.D. The effect of the SiO_2/Na_2O ratio in the structural modification of metakaolin-based geopolymers studied by XRD, FTIR and MAS-NMR. *J. Ceram. Sci. Technol.* **2014**, *5*, 185–191. [CrossRef]
94. Garcia-Lodeiro, I.; Palomo, A.; Fernández-Jiménez, A.; MacPhee, D.E.E. Compatibility studies between N-A-S-H and C-A-S-H gels. Study in the ternary diagram Na_2O–CaO–Al_2O_3–SiO_2–H_2O. *Cem. Concr. Res.* **2011**, *41*, 923–931. [CrossRef]
95. Bernal, S.A.; Provis, J.L.; Rose, V.; Mejía De Gutierrez, R. Evolution of binder structure in sodium silicate-activated slag-metakaolin blends. *Cem. Concr. Compos.* **2011**, *33*, 46–54. [CrossRef]

96. Puertas, F.; Martínez-Ramírez, S.; Alonso, S.; Vázquez, T. Alkali-activated fly ash/slag cements. *Cem. Concr. Res.* **2000**, *30*, 1625–1632. [CrossRef]
97. Kaze, C.R.; Jiofack, S.B.K.; Cengiz, Ö.; Alomayri, T.S.; Adesina, A.; Rahier, H. Reactivity and mechanical performance of geopolymer binders from metakaolin/meta-halloysite blends. *Constr. Build. Mater.* **2022**, *336*, 127546. [CrossRef]
98. Rodrigue Kaze, C.; Adesina, A.; Alomayri, T.; Assaedi, H.; Kamseu, E.; Chinje Melo, U.; Leonelli, C. Characterization, reactivity and rheological behaviour of metakaolin and Meta-halloysite based geopolymer binders. *Clean. Mater.* **2021**, *2*, 100025. [CrossRef]
99. Azevedo, A.R.G.; Vieira, C.M.F.; Ferreira, W.M.; Faria, K.C.P.; Pedroti, L.G.; Mendes, B.C. Potential use of ceramic waste as precursor in the geopolymerization reaction for the production of ceramic roof tiles. *J. Build. Eng.* **2020**, *29*, 101156. [CrossRef]
100. Lu, C.; Zhang, Z.; Shi, C.; Li, N.; Jiao, D.; Yuan, Q. Rheology of alkali-activated materials: A review. *Cem. Concr. Compos.* **2021**, *121*, 104061. [CrossRef]

Disclaimer/Publisher's Note: The statements, opinions and data contained in all publications are solely those of the individual author(s) and contributor(s) and not of MDPI and/or the editor(s). MDPI and/or the editor(s) disclaim responsibility for any injury to people or property resulting from any ideas, methods, instructions or products referred to in the content.